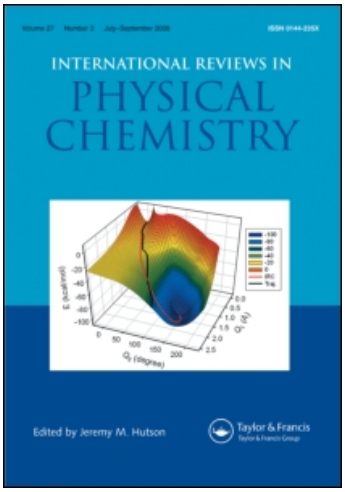

International Reviews in Physical Chemistry
Publication details, including instructions for authors and subscription information:
http://www.informaworld.com/smpp/title~content=t713724383

Time correlation function and its unifying role in molecular structure and dynamics

S. Mahapatra; N. Chakrabarti; N. Sathyamurthy

Online publication date: 26 November 2010

To cite this Article Mahapatra, S. , Chakrabarti, N. and Sathyamurthy, N.(1999) 'Time correlation function and its unifying role in molecular structure and dynamics', International Reviews in Physical Chemistry, 18: 2, 235 — 262
To link to this Article: DOI: 10.1080/014423599229956
URL: http://dx.doi.org/10.1080/014423599229956

INTERNATIONAL REVIEWS IN PHYSICAL CHEMISTRY, 1999, VOL. 18. NO. 2, 235–262

Time correlation function and its unifying role in molecular structure and dynamics

S. MAHAPATRA†, N. CHAKRABARTI‡ and N. SATHYAMURTHY§‖
Department of Chemistry, Indian Institute of Technology, Kanpur 208 016, India

The utility of time correlation functions computed by time evolving suitably chosen wave packets to studies of bound states of molecules, quasibound states and transition state resonances in reactive systems, photoabsorption–dissociation and resonance Raman scattering in molecules is illustrated using examples from our own laboratory. The role of excited electronic states and wavefunction interference effects in influencing photoexcitation observables is examined using model systems.

1. Introduction

The concept of the time correlation function is amazingly simple but highly powerful. It is used in classical mechanics and also in quantum mechanics. It can be used for an isolated system as well as a system under external influence. It can be used for a variety of observables. Although the early use of time correlation functions in spectroscopy could be traced back to the 1940s [1, 2] and the utility of time correlation functions has been well documented in the literature in the 1960s [3], much of the credit for the resurgence in activity in the area should perhaps go to Heller [4, 5]. From a practical point of view, developments in computational hardware (speed and memory) and in the practice of time-dependent quantum-mechanical (TDQM) methodology [6–11] and experiments in probing ultrafast phenomena [12, 13] have been responsible for the mushroom growth in the literature on time correlation functions in recent years.

In this review, we concern ourselves with the wavefunction time correlation function and its application to a study of molecular structure and dynamics in elementary chemical systems. The correlation function could be an autocorrelation function or a cross-correlation function. The autocorrelation function $C(t)$ is defined as the scalar product of the wavefunction Ψ at any time t with its initial ($t = 0$) value:

$$C(t) = \langle \Psi(0) | \Psi(t) \rangle. \tag{1}$$

$C(t)$ is invariably complex but $|C(t)|^2$ is always real and positive and is referred to as the survival probability $P(t)$. The Fourier transform of $C(t)$ takes it to the frequency domain [14]. For an isolated system evolving in time on a single potential energy surface, for example, the Fourier transform of $C(t)$ yields the eigenvalue spectrum:

$$I(E) = \left| \int_{-\infty}^{\infty} \exp\left(\frac{iEt}{\hbar}\right) C(t)\, dt \right|^2. \tag{2}$$

† Present address: Theoretische Chemie, Physikalisch-Chemisches Institut, Universität Heidelberg, Im Neuenheimer Feld 253, D-69120 Heidelberg, Germany.
‡ Present address: Département de Chimie, Université de Montréal, C.P. 6128, Succursale Centre-Ville, Montréal (Québec), Canada H3C 3J7.
§ S.N. Bose National Centre for Basic Sciences, Calcutta, India.
‖ Email: nsath@iitk.ac.in

International Reviews in Physical Chemistry ISSN 0144–235X print/ISSN 1366–591X online © 1999 Taylor & Francis Ltd
http://www.tandf.co.uk/JNLS/rpc.htm http://www.taylorandfrancis.com/JNLS/rpc.htm

If the initial wavefunction represented a pure state, then $C(t)$ would be a periodic function of t, and $I(E)$ would be a δ function centred at the eigenvalue of the state. However, if $\Psi(0)$ represented a superposition of states, it can be shown readily that the power spectrum (2) would consist of spectral lines of varying intensity, corresponding to different eigenstates E_n of various weightages. The eigenfunctions $\Psi(E_n)$ of the non-degenerate eigenstates would be obtained by projecting the components out of the time-evolved wavefunction:

$$\Psi(E_n) = \int_{-\infty}^{+\infty} \Psi(t) \exp\left(\frac{\mathrm{i}E_n t}{\hbar}\right) \mathrm{d}t. \tag{3}$$

In practice, the integrals in equations (2) and (3) cannot be carried over time varying from $-\infty$ to $+\infty$, but over a finite interval from 0 to T. In order to correct for this finite range of t, it is common to include a window function $w(t)/T$ [15], such that

$$I(E) = \left| \frac{1}{T} \int_0^T C(t) w(t) \exp\left(\frac{\mathrm{i}Et}{\hbar}\right) \mathrm{d}t \right|^2 \tag{4}$$

and

$$\Psi(E_n) = \frac{1}{T} \int_0^T \Psi(t) w(t) \exp\left(\frac{\mathrm{i}E_n t}{\hbar}\right) \mathrm{d}t. \tag{5}$$

It is common to use a Hanning window function [16]:

$$w(t) = \begin{cases} 1 - \cos\left(\dfrac{2\pi t}{T}\right) & \text{if } 0 \leqslant t \leqslant T, \\ 0 & \text{if } t > T, \end{cases} \tag{6}$$

although other alternatives exist [17, 18].

For a bound state problem, thus, one can compute the eigenfunctions and eigenvalues by computing the autocorrelation function for a single wave packet (WP) evolving in time. Depending upon the choice of $\Psi(0)$, some of the eigenstates may be missed out, but they can be resolved from $C(t)$ obtained for a different choice of $\Psi(0)$.

For collisional systems involving no bound states but possibly quasibound states, which would be manifested as resonances in the plots of the reaction probability P^R against the energy, the autocorrelation function can be used to compute the eigenvalues corresponding to the quasibound states and hence to predict resonances. The nature of the resonances and their lifetimes could be discerned by computing the eigenfunctions and the spectral line shapes respectively.

The pioneering work of Heller and co-workers [4, 5, 19–22] in the late 1970s and early 1980s opened up an exciting area of research called WP spectroscopy. Their approach utilizes time correlation function as the central quantity in real-time investigation of dynamical events occurring on a femtosecond time scale. Interaction of light with a single gas molecule comes under the study of photon-driven dynamics [23–27]. In investigations of the dynamical processes initiated by photon(s), the dynamics involve more than one electronic state. For a two-state system, for example, the absorption spectrum can be computed from the autocorrelation function [23]. For a system in the vibrational state $|i\rangle$ of the ground electronic state, let the nuclear wavefunction at time $t = 0$ be represented by $\Psi_i(0)$. On optical excitation, the

wavefunction $\Phi_i(0)$ (referred to as the promoted-state wavefunction) on the excited state would become [28]

$$\Phi_i(0) = \mu \cdot \boldsymbol{E} \Psi_i(0), \tag{7}$$

where μ is the transition dipole vector and $\boldsymbol{E}$ represents the electric field of the photon. The time evolution of the wavefunction would now be governed by the excited-state Hamiltonian H_{ex}, and $\Phi_i(t)$ would be obtained from

$$\Phi_i(t) = \exp\left(-\frac{\mathrm{i}H_{ex}\, t}{\hbar} \right) \Phi_i(0). \tag{8}$$

The autocorrelation function $C_{ii}(t)$ for the system would then be

$$C_{ii}(t) = \langle \Phi_i(0) \,|\, \Phi_i(t) \rangle. \tag{9}$$

The absorption spectrum would be computed from $C_{ii}(t)$ as [5, 19, 27]

$$\sigma_A(\omega) = \frac{2\pi\omega}{3\hbar c} \int_{-\infty}^{+\infty} C_{ii}(t) \exp\left(\frac{\mathrm{i}Et}{\hbar} \right) \mathrm{d}t, \tag{10}$$

where ω is the frequency of the incident radiation and $E = E_g + \hbar\omega$, with E_g the internal energy of the molecule in its ground electronic state. If the excited state is a dissociative state, the photoabsorption–dissociation cross-section would be structureless, except to mirror the nodal structure of the vibrational wavefunction of the ground electronic state. In the case when the excited state is also a bound state, the absorption spectrum would consist of a set of lines corresponding to the eigenvalue spectrum of the excited state.

The emission spectrum from an excited state of a system can be computed by reversing the roles of the ground and excited states. For example, Mahapatra and Köppel [29] have computed the optical emission spectra of Rydberg-excited H_3 and its isotopomers from their third principal quantum shell to the degenerate ground electronic manifold and compared with the experimental recording recently.

When the overlap between the time-evolved promoted-state wavefunction $\Phi_i(t)$ and the wavefunction ($\Phi_f = \mu \cdot \boldsymbol{E} \Psi_f$) corresponding to the vibrational state f of the ground electronic state is computed, we obtain the cross-correlation function:

$$C_{fi}(t) = \langle \Phi_f \,|\, \Phi_i(t) \rangle. \tag{11}$$

This is often called the Raman correlation function. The half-Fourier transform of $C_{fi}(t)$ yields the Raman amplitude

$$\alpha_{fi}(\omega) = \frac{\mathrm{i}}{\hbar} \int_0^{\infty} C_{fi}(t) \exp\left[\mathrm{i}(\omega + \omega_i)t \right] \mathrm{d}t. \tag{12}$$

The 'observable' Raman scattering intensity $I_{fi}(\omega)$ (also called the 'Raman excitation profile') is proportional to the squared modulus of the Raman amplitude [5, 20]:

$$I_{fi}(\omega) \propto \omega\omega_s^3 |\alpha_{fi}(\omega)|^2, \tag{13}$$

where ω_s is the frequency of the scattered radiation. If $f = i = 0$, then $I_{fi}(\omega)$ is the Rayleigh scattering intensity. When $i = 0, f = 1$, then $I_{fi}(\omega)$ refers to the fundamental (Stokes) Raman transition and, when $i = 1, f = 0$, it would correspond to the anti-Stokes line. The overtones of the Stokes–Raman emission would correspond to $i = 0$, $f = 2, 3, \ldots$, etc. For an extensive review of the literature on the utility of cross-

correlation functions to resonance Raman investigations of a variety of systems, the reader is referred to [30].

One of the advantages of the time correlation function is that it portrays the nature of the dynamical system right away. For a bound state there would be characteristic recurrences revealing the time period of the WP motion. In the case of a repulsive state, $C(t)$ would be a decaying function, the decay rate depending on the steepness of the repulsive potential. In the case when the system supports a number of quasibound states, there would be several oscillations in the plot of $C(t)$, revealing several frequency components. Interferences between wavefunctions evolving on two or more coupled electronic states will also be evident from $C(t)$ plots.

The key to computing the time correlation function is to evolve the wavefunction of a system for a desired length of time. The computational methodology for the same has been dealt with in detail elsewhere [10]. In this review we focus attention only on obtaining valuable insight into molecular structure and dynamics from the computed $C(t)$. By no means do we claim to cover the entire $C(t)$ literature in this review. An extensive list of references to its utility in photoexcitation processes can be found in [10]. Because of space and time restrictions, we confine ourselves to a discussion of a few topics that are directly related to the work done in our laboratory.

We highlight some of the applications to the bound-state problem in section 2, and the quasibound states and transition-state resonances in section 3. An analysis of the nature (regular or irregular) of the resulting spectra is presented in section 4. Using model diatomic potentials, we illustrate the use of autocorrelation and cross-correlation functions in the study of photoexcitation processes involving single electronic excited states in section 5.1. Interference effects arising from multiple excited electronic states are discussed in section 5.2. The problem of recovery of cross-correlation functions from the Raman excitation profiles is highlighted in section 5.3. That is followed by a summary and conclusion section 6.

2. Bound states

The basic methodology in computing the eigenvalues and eigenfunctions of bound states supported by potentials with one or more minima using time correlation functions has already been outlined in the introduction. It can be carried out easily for diatomic systems [31–33]. Its utility for triatomic molecules was demonstrated long ago [15]. More recently, we have obtained the bound states for collinear HeH_2^+ [34] and its isotopic variants [35], and also for a model Pt–NO system [36]. Very recently, we have computed the bound states for three-dimensional HeH_2^+ and $HeHD^+$ [37]. Still, it is not the method of choice for many systems, particularly if the system involves more than three degrees of freedom, and/or there are degenerate states.

There are systems for which the $C(t)$ route is particularly suited when it comes to studying the bound states. A case in point is H_3^+ for which experiments showed that there were about 27000 well resolved transitions in a 220 cm^{-1} region of the photodissociation spectrum [38–40]. It would be difficult to use any of the conventional methods to arrive at the bound states of this system. Evaluation of $C(t)$ for different lengths of time enabled Garcia de Polavieja *et al.* [41] to compute the spectrum at different levels of resolution. Short-time dynamics could reveal the gross features and the regularity in the spectrum while the long-time dynamics revealed the additional lines and the irregularity therein. In fact, the method has been used to characterize the eigenfunctions corresponding to motions of 'horseshoe' and 'elephant foot' variety of chaos in the intramolecular dynamics of H_3^+.

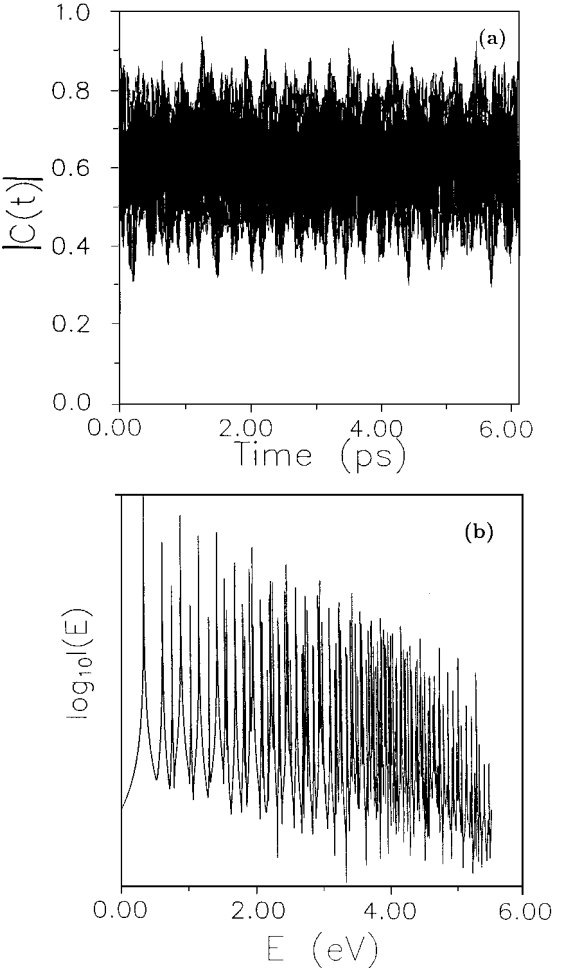

Figure 1. (*a*) Variation in the magnitude of the time correlation function $|C(t)|$ showing the bound nature of collinear N_2H^+. (*b*) Energy eigenvalue spectrum obtained by Fourier transforming the above time correlation function. The peaks in the spectrum correspond to the vibrational energy levels in collinear N_2H^+.

Recently, Mahapatra *et al.* [42] have followed the time correlation function approach to identify a large number of bound states for N_2H^+ in collinear as well as three-dimensional geometries. The procedure involved is the following: choose a WP with a certain average energy $\langle E \rangle$ located initially ($t = 0$) in the interaction region, follow its time evolution by solving numerically the time-dependent Schrödinger equation on a grid in Jacobi coordinate space and compute the time correlation function over the entire duration. The technical details of the calculation have been given elsewhere [42]. The result $|C(t)|$ for an initial WP with $\langle E \rangle = 0.7128$ eV for collinear N_2H^+ is reproduced in figure 1 (*a*). It can be seen that, except for an initial decline due to the dephasing of the initial WP, $|C(t)|$ is dominated by recurrences persisting over the entire time scale. This is typical of $|C(t)|$ for a bound system. The recurrence pattern in figure 1 (*a*) clearly indicates that it results from a large number of states with various frequencies. The energy eigenvalue spectrum obtained by Fourier transforming the above autocorrelation function is reproduced in figure 1 (*b*), where

the intensity is plotted on a logarithmic scale as a function of energy. The peak positions in the spectrum correspond to the bound states of collinear N_2H^+. The energy resolution of the spectrum is 6.7×10^{-4} eV corresponding to a total of 6.18 ps evolution of the WP. Although the spectrum is well resolved at lower energies, the peaks overlap at higher energies owing to a large increase in the energy level density. By choosing higher-energy initial WPs and longer propagation times a large number of these levels at higher energies has been resolved, although there are many degenerate or near-degenerate levels which are not obtained by this route. In section 4 we shall show that the extent of complexity in such a spectrum can be estimated quantitatively by analysing the survival probability $P(t)$ averaged over the initial state and the Hamiltonian.

Mahapatra and Köppel [43] have recently computed the bound states of the upper adiabatic sheet of the degenerate ground electronic manifold of H_3 using the $C(t)$ route. These bound states change over to resonances and decay with 3–6 fs when the non-adiabatic coupling is included. The existence of 'horseshoe' states on the lower adiabatic sheet at the perpendicular geometry of H_3 and their instability in three dimensions has also been reported by these workers.

3. Quasibound states and transition-state resonances

Investigation of the plots of reaction probability as a function of energy for many atom–diatom systems reveals a number of oscillations that can be characterized as reactive scattering resonances. While some of them could be identified as shape resonances and some as threshold or barrier resonances, many of them are of Feshbach (compound state) type, arising from bound states supported by vibrational adiabatic potentials. Several of them cannot be classified as any of the above and they can be related to unstable periodic orbits in a classical-mechanical description and can carry the signature of classical or quantum chaos. The autocorrelation function approach is well suited to a study of such resonances and the quasibound states associated with them. A suitably chosen WP in the interaction region (in the vicinity of the transition state, for example) is time evolved until most of it leaves the interaction region and $C(t)$ is calculated for the entire time period. Fourier transform of the latter yields a pseudospectrum, the peaks of which are centred at the eigenvalues corresponding to the different quasibound states. The corresponding eigenfunctions can be computed as described earlier and they provide valuable insight into the nature of the transition state. The spectral line shapes are indicative of the nature of the resonances and they can be inferred readily (see below).

The method has been applied to a study of transition state resonances in collinear and three-dimensional $H+H_2$ [44, 45], $D+H_2$ [46], $He+H_2^+$ [34, 37], $He+HD^+$ (DH^+) [35], H^-+H_2 [47] and $\mu+H_2$, D_2 [48] collisions in recent years. We illustrate the methodology and the insight obtained using collinear (He, H_2^+) as a test case.

The initial wavefunction $\Psi(R, r, t = 0)$ was taken as an even-parity Gaussian wave packet (GWP) in terms of He—H and H—H bond distances r_{He-H} and r_{H-H} respectively:

$$\Psi(R, r, t = 0) = N\exp\left(-\frac{(r_{He-H}-r^0_{He-H})^2}{2\delta^2}-\frac{(r_{H-H}-r^0_{H-H})^2}{2\delta^2}\right), \tag{14}$$

where N is the normalization constant, r^0_{He-H} and r^0_{H-H} specify the initial location of

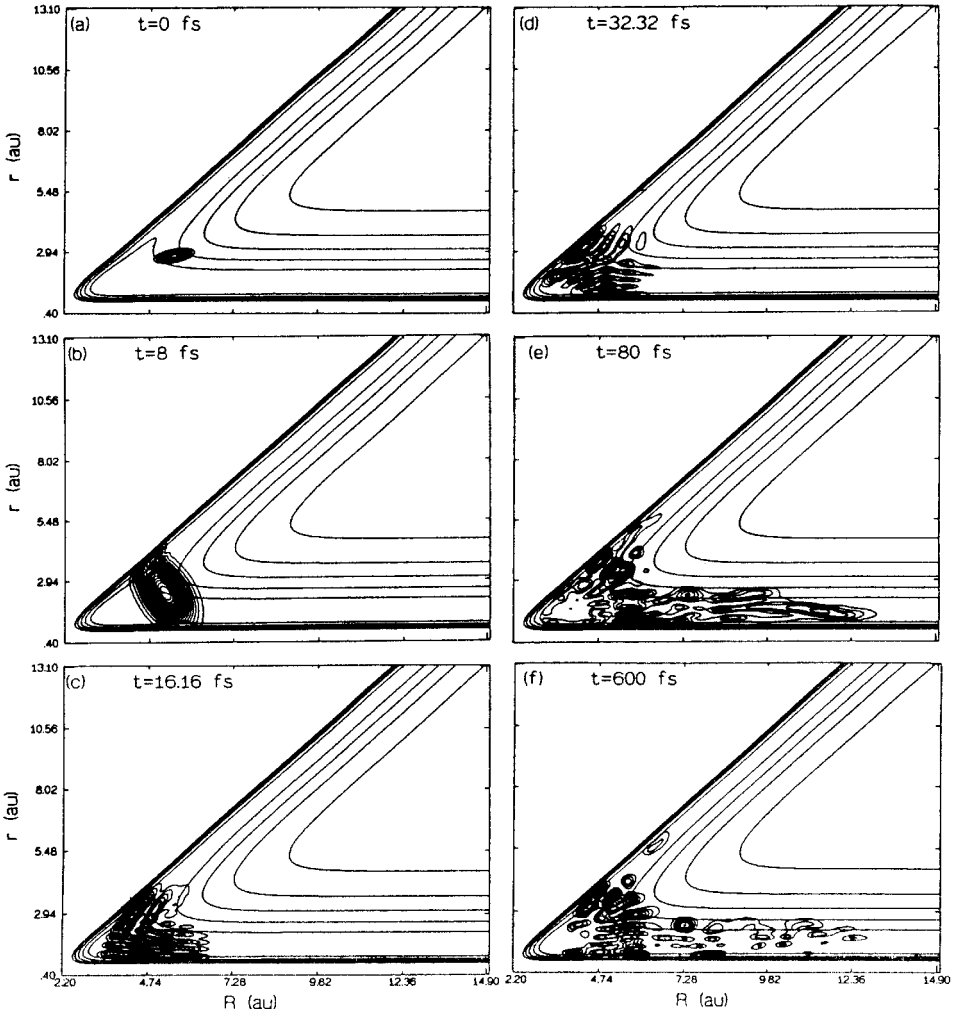

Figure 2. Probability density contours of the initial GWP with $\langle E \rangle = 0.9924$ eV and width $\delta = 0.25a_0$ at the different times indicated, showing its evolution on a 256× 256 potential grid. The total probability densities of the WP retained on the grid at different times are 1.0, 1.0, 0.99, 0.99, 0.77 and 0.035 in (*a*), (*b*), (*c*), (*d*), (*e*) and (*f*) respectively. An optical potential has been used to remove the part of the wavefunction that reaches the grid edges.

the centre of the WP and δ is the width parameter. R and r are the Jacobi coordinates related to $r_{\mathrm{He-H}}$ and $r_{\mathrm{H-H}}$ through

$$r_{\mathrm{He-H}} = dR - \frac{r_{\mathrm{H-H}}}{2} \tag{15}$$

and

$$r_{\mathrm{H-H}} = d^{-1} r, \tag{16}$$

where d is the scaling parameter given by the square root of the ratio of the reduced mass of H_2^+ to the three-body reduced mass $\mu = [m_{\mathrm{He}}\, m_{\mathrm{H}}\, m_{\mathrm{H}} / (m_{\mathrm{He}} + m_{\mathrm{H}} + m_{\mathrm{H}})]^{1/2}$.

The time evolution of the WP was followed on a 256× 256 grid in (R, r) space with

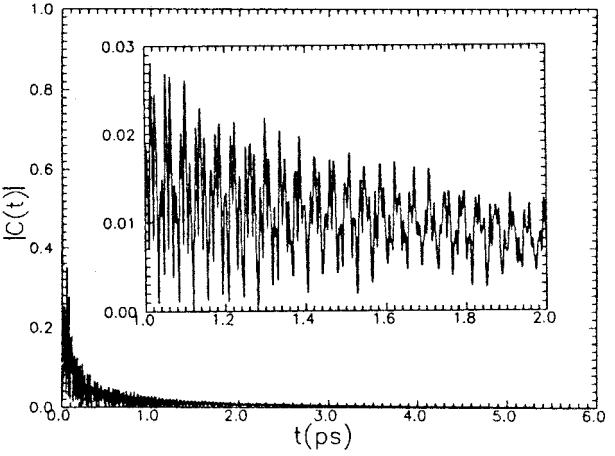

Figure 3. The decay of the absolute value of the autocorrelation function for the GWP depicted in figure 2. The portion of the curve for $t = 1$–2 ps is magnified and shown in the inset.

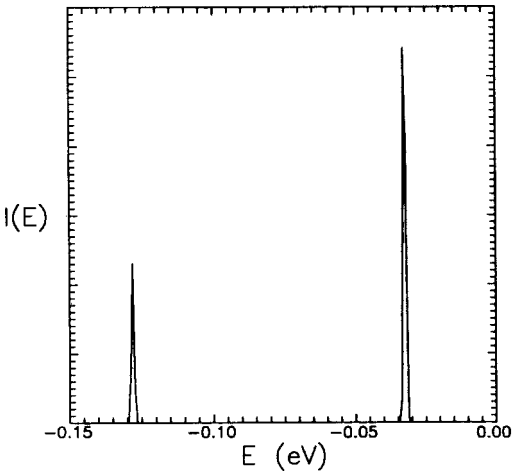

Figure 4. The eigenvalue spectrum corresponding to the bound states of collinear HeH_2^+, computed from the autocorrelation function in figure 3.

the origin at $(2.2, 0.4)a_0$ and increments $\Delta R = \Delta r = 0.05a_0$ using the split operator method [15] for successive time intervals Δt of 0.1616 fs each, amounting to a total of 5.29 ps.

For a particular choice of initial GWP centred at $(R^0, r^0) = (5.422, 2.793)a_0$ with $\langle E \rangle = 0.9924$ eV, the time evolution is shown in terms of probability density contours superimposed on the potential energy contour diagram at different times in figure 2. It is clear from the decay of $|C(t)|$ reproduced in figure 3 that there are a large number of recurrences and that, even after several picoseconds, there is a small part of the wavefunction that lingers on in the interaction region, implying that some of the quasibound states of collinear HeH_2^+ have lifetimes greater than a few picoseconds.

It can be seen from the power spectra shown in figures 4 and 5 that there are two bound states and a large number of quasibound states and hence resonances for the system. By fitting individual spectral lines of figure 5 to a Lorentzian we obtain lifetimes of some of the quasibound states as much as approximately 1.9 ps.

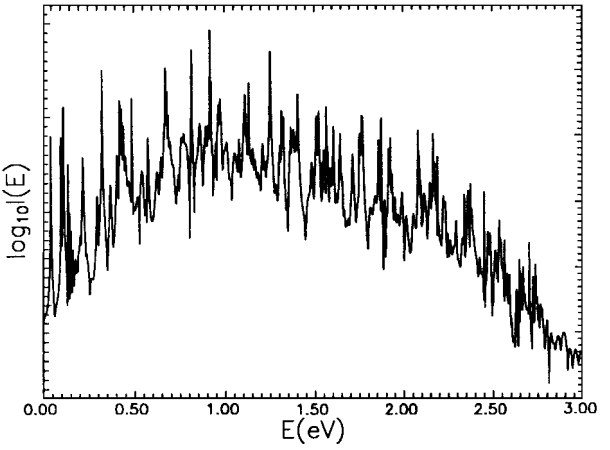

Figure 5. The eigenvalue spectrum corresponding to the quasibound states of collinear HeH_2^+, computed from the autocorrelation function in figure 3.

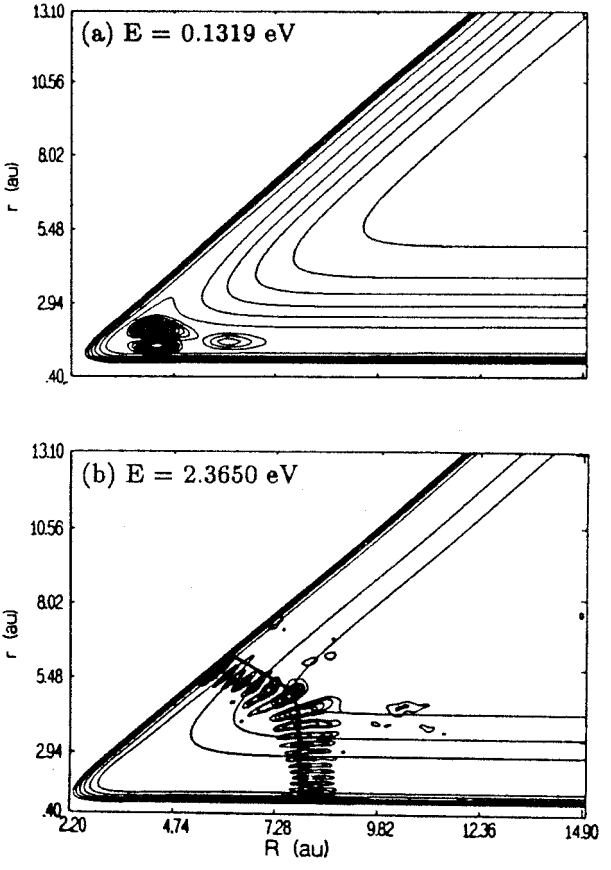

Figure 6. Probability density contours superimposed on the potential grid for two resonance wavefunctions. The eigenenergies are indicated. The closely lying resonant periodic orbit at 2.3650 eV is superimposed on the corresponding resonance eigenfunction, to illustrate the classical-quantal correspondence.

An examination of the eigenfunctions corresponding to the different eigenvalues reveals that at low energies they correspond to local modes and that at higher energies they are hyperspherical in nature as illustrated in figures 6(*a*) and (*b*) respectively. The latter figure includes the corresponding resonant periodic orbit at that energy. An extensive analysis of the stable and unstable periodic orbits and their relationship to the quasibound state eigenfunctions of collinear HeH_2^+ has been given elsewhere [49].

4. Spectral analysis

Although the eigenfunctions of the quasibound states in figure 5 can be identified from their characteristic nodal pattern at low and moderate energies and can be assigned in terms of quantum numbers, they exhibit complex nodal patterns that are difficult to assign at higher energies. The difficulty is connected with the increasing level density at higher energies and strong coupling between various molecular modes of motion. This brings out many interesting and specific features in the dynamics, which are not observed in the low-energy regime. There can be no good quantum numbers for the system when the different modes are coupled with each other. The complexity in the energy spectrum is also reflected in the recurrence pattern of $|C(t)|$. However, a quantitative estimate of this complexity can be obtained from the survival probability $\langle\langle P(t)\rangle\rangle$ averaged over the initial states and the Hamiltonian of the system. This quantity in conjunction with the analytical predictions of random matrix theory (RMT) uniquely identifies the irregularity in the system originating from the mode coupling.

The ensemble-averaged survival probability $\langle\langle P(t)\rangle\rangle$ can be computed by Fourier transforming the spectral autocorrelation function $G(\omega)$ [50], followed by averaging over the initial states and the Hamiltonian. Therefore, it can also be used to extract information from an experimental recording. Furthermore, it is particularly suitable for analysing spectra of poor resolution. In terms of the energy eigenvalues, the survival probability $\langle P(t)\rangle$ averaged over the initial states is given by [51]

$$\langle P(t)\rangle = \frac{3}{N+2}\left[1 + \frac{2}{3N}\sum_{n,m;n>m}\cos\left(2\pi(\bar{E}_n - \bar{E}_m)\frac{t}{\langle\Delta E\rangle}\right)\right], \tag{17}$$

where $\langle\Delta\bar{E}\rangle$ is the average energy spacing in the spectrum. In practice the raw energy level spectrum is first unfolded [52] with respect to a constant average energy level spacing and the new set of scaled energy levels $\bar{E}_i$ are calculated. This removes the irrelevant secular variation in the level spacings (a decrease in the spacing with increase in energy for a Morse oscillator, for example) from the spectrum keeping their fluctuation variation unaffected. To obtain $\langle\langle P(t)\rangle\rangle$ the quantity in equation (17) is further averaged over n levels which are grouped into several segments, each containing N levels (averaging over the Hamiltonian). In the case of a regular spectrum, $\langle\langle P(t)\rangle\rangle$ starts from an initial value of 1.0 and monotonically approaches the asymptotic value of $3/(N+2)$. On the other hand, for an irregular spectrum, $\langle\langle P(t)\rangle\rangle$ falls below its asymptotic value at short times ($t = 2\pi\hbar/\langle\Delta\bar{E}\rangle$) and approaches the asymptotic limit at later times. The dip below the asymptotic value at short times is termed the 'correlation hole', which is a graphic evidence of the level repulsion in the case of an irregular spectrum. The $\langle\langle P(t)\rangle\rangle$ values obtained from the quasibound states of collinear HeH_2^+ are shown as a solid curve in figure 7 [53]. The dip in $\langle\langle P(t)\rangle\rangle$ below the asymptotic line clearly emphasizes the signature of the underlying irregularity in the quasibound spectrum of HeH_2^+.

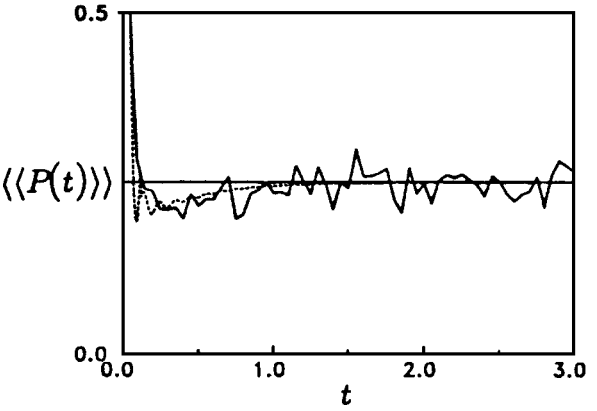

Figure 7. Variation in the ensemble-averaged survival probability $\langle\langle P(t)\rangle\rangle$ with time t (in arbitrary units) for the quasibound states spectrum of collinear HeH_2^+, plotted as a solid curve. $\langle\langle P(t)\rangle\rangle$ values derived from the RMT for $\beta = 0.6$ are shown as a broken curve.

The extent of irregularity is estimated by comparing the $\langle\langle P(t)\rangle\rangle$ values with those predicted by the RMT. The latter are given by [54]

$$\langle\langle P(t)\rangle\rangle = \frac{3}{N+2}\{1 + \Delta_N * [\delta(\tau) - b_{2\beta}(\tau)]\}, \tag{18}$$

where $\tau = t/2\pi\langle\rho\rangle$, with $\langle\rho\rangle$ as the average level density. $b_{2\beta}(t)$ is the two-level form factor obtained by Fourier transforming the two-point cluster function $Y_{2\beta}(\omega)$ [55]. If a fraction β of the levels obey Guassian orthogonal ensemble (irregular) statistics and $1-\beta$ obey Poisson (regular) statistics, then $b_{2\beta}(t)$ is given by

$$b_{2\beta}(t) = \beta b_2\left(\frac{t}{\beta}\right) + \frac{(1-\beta)}{N}\delta(t). \tag{19}$$

The asterisk in equation (18) implies a convolution and $\Delta_N = N^{-1}\{[\sin(\pi N t)]/\pi t\}^2$. The preceding two equations imply that the δ function governs the short-time behaviour of $\langle\langle P(t)\rangle\rangle$ and the subsequent long-time behaviour resulting in the dip below the asymptotic limit is governed by $b_2(t)$. The broken curve shown in figure 7 is obtained for a value of $\beta = 0.6$ implying that about 60% of the quasibound states of collinear HeH_2^+ contribute to its irregular dynamical behaviour. We have also calculated $\langle\langle P(t)\rangle\rangle$ for collinear $HeHD^+$ and $HeDH^+$ and found about 90% of the quasibound states of the former and about 20% of the latter to contribute to their irregular dynamical behaviour [56]. $\langle\langle P(t)\rangle\rangle$ calculated from the bound state spectrum of collinear N_2H^+ revealed about 75% irregularity in its dynamics [42]. A similar analysis of the bound states and resonances for HO_2 [57] revealed about 90% irregularity in this system, in accord with other classical and quantal measures of irregularity.

5. Photoexcitation processes

5.1. *Model diatoms: single excited state*

In order to illustrate the basic methodology in computing photoabsorption–dissociation cross-sections and resonance Raman scattering intensities we have carried out dynamical calculations on four different model diatomic molecular systems undergoing photoexcitation and subsequent emission.

We have considered a harmonic ground-electronic-state potential energy curve

$$V^{g}_{HO} = \tfrac{1}{2}k_g(r - r_e)^2 \tag{20}$$

and four different excited-state potential energy curves: dissociative (indicated by the subscript DIS), harmonic (indicated by the subscript HO), Morse oscillator (indicated by the subscript MO) and symmetric double well (indicated by the subscript SDW) in nature. The corresponding functional forms are:

$$V^{e}_{DIS} = a\exp[-b(r - r_1)] + c_1, \tag{21}$$

$$V^{e}_{HO} = \tfrac{1}{2}k_e(r - r_2)^2 + c_2, \tag{22}$$

$$V^{e}_{MO} = D_e\{1 - \exp[-\alpha(r - r_3)]\}^2 + c_3, \tag{23}$$

$$V^{e}_{SDW} = \tfrac{1}{2}k_1(r - r_4)^2 + \tfrac{1}{2}k_2(r - r_4)^4 + v_b\exp[-d(r - r_4)^2] + c_4. \tag{24}$$

The parameters defining the harmonic ground state and the four excited states corresponding to the four different model systems are listed in table 1. The potential energy curves for the different model systems are shown in figure 8.

We have performed the WP dynamical calculations by combining a second-order differencing (SOD) scheme for temporal evolution and a fast Fourier transform (FFT) algorithm for spatial evolution on a one-dimensional grid in r. At $t = 0$ the WP $\chi(0)$ represents the ground-vibrational-state wavefunction on the ground electronic state and a Franck–Condon (FC) transition takes it to the excited electronic state:

$$|\phi(0)\rangle = \mu|\chi_0\rangle. \tag{25}$$

The transition dipole moment μ has been taken to be coordinate independent (the Condon approximation) and is equated to unity in the present study. The propagation of the 'promoted-state wavefunction', $\phi(0)$, is carried out on the excited state under the action of the excited state Hamiltonian H_{ex} [6]:

$$\phi(t + \Delta t) = \phi(t - \Delta t) - \frac{2iH_{ex}\,\Delta t}{\hbar}\phi(t), \tag{26}$$

where Δt is the time step used in time evolution. The overlap of the initial 'promoted state' $\phi(t = 0)$ with its time-evolved form $\phi(t)$ is computed to obtain the auto-correlation function $C_{00}(t)$ at every time step of propagation. The absorption cross-section [4, 19] is computed using equation (10).

Evaluation of the overlap of the time-evolved promoted state $\phi(t)$ at each time step with another promoted state $\phi_1 (= \mu\chi_1)$ corresponding to the $v = 1$ eigenfunction χ_1 of the ground electronic state yields the cross-correlation function $C_{10}(t)$, the half-Fourier transform of which yields the Raman amplitude (equation (12)) and the Raman intensity (equation (13)).

The nature of the excited state is reflected in the autocorrelation (cross-correlation) function and naturally in the absorption spectrum (Raman excitation profile).

It is worth pointing out that the basic ideas used in this section are similar to those utilized in sections 2 and 3 on bound and quasibound states. The main difference is that we dealt with pseudospectra in earlier sections while we deal with 'real' spectra in the present section.

5.1.1. *Harmonic excited state*

The WP propagation on the excited state was carried out on a spatial grid $(r_{min}, dr, N_r) = (3.5a_0, 0.05a_0, 128)$ for a total of 352.91 fs using $\Delta t = 0.01077$ fs. The promoted-state wavefunction revisits the FC region periodically because of the bound nature of

Table 1. Parameters for the model potential energy curves.

k_g, r_e	3.0 eV a_0^{-2}, $6.0a_0$
a, b, r_1, c_1	3.0 eV, $0.3a_0^{-1}$, $3.5a_0$, 4.62 eV
k_e, r_2, c_2	3.0 eV a_0^{-2}, $6.5a_0$, 2.7 eV
D_e, r_3, α, c_3	2.5 eV, $6.3a_0$, $0.7a_0^{-1}$, 2.9 eV
$k_1, k_2, V_b, d, r_4, c_4$	3.0 eV a_0^{-2}, 0.2 eV a_0^{-4}, 0.5 eV, $10.0a_0^{-2}$, $6.8a_0$, 1.998 eV

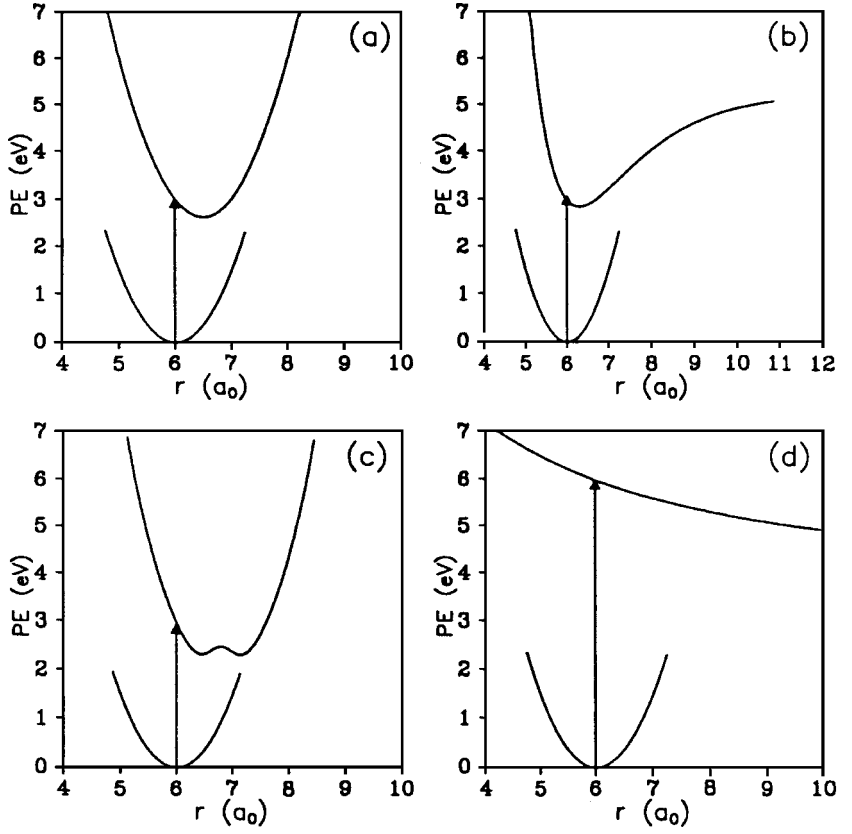

Figure 8. The potential energy (PE) curves for (*a*) harmonic-to-harmonic, (*b*) harmonic-to-Morse, (*c*) harmonic-to-symmetric double-well and (*d*) harmonic-to-dissociative excitations.

the excited state. The autocorrelation function is a periodically oscillating function of time and the height of the peaks in $C_{00}(t)$ remains the same throughout the time span as can be seen in figure 9(*a*). The absorption cross-section (figure 9(*b*)) shows structures which are correlated to the vibrational levels of the excited state. The cross-correlation function $C_{10}(t)$ also shows (figure 9(*c*)) periodicity and, within each crest, dips are indicative of the nodal pattern of the final-state wavefunction. The height of the crests in $C_{10}(t)$ also remains the same at all times as we have not introduced the phenomenological damping factor Γ. The Raman excitation profile (REP) also shows structures corresponding to the vibrational levels of the excited state.

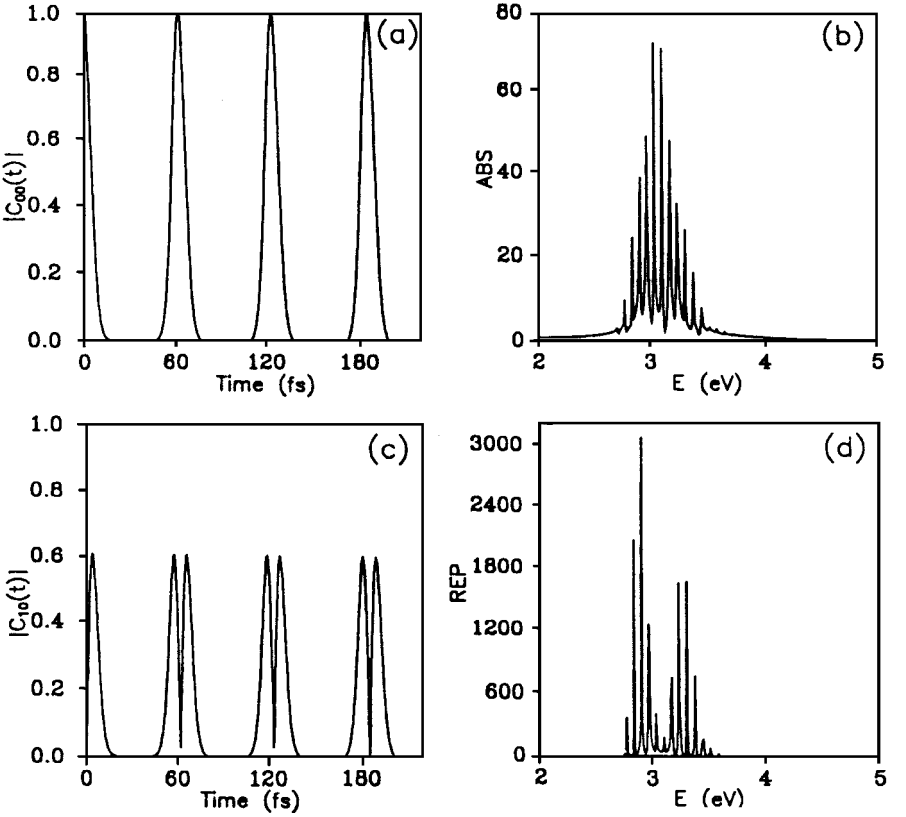

Figure 9. (*a*) The autocorrelation function, (*b*) the absorption (ABS) cross-section, (*c*) the cross-correlation function and (*d*) the REP for harmonic-to-harmonic excitation.

5.1.2. *Morse excited state*

The WP propagation on the Morse excited state was carried out on a spatial grid $(r_{\min}, \mathrm{d}r, N_r) = (4.5a_0, 0.05a_0, 128)$ for a total of 352.91 fs using $\Delta t = 0.01077$ fs. The region close to the zero-point energy level of the Morse potential is close to that of the harmonic potential but the anharmonicity increases with increase in energy. The autocorrelation and cross-correlation functions (shown in figures 10(*a*) and (*c*)) are less symmetric in harmonic-to-Morse type of excitation than in harmonic-to-harmonic transitions. Since in the Morse potential the wall supporting the inner turning point is more repulsive than the wall supporting the outer turning point, the probability of locating the particle around the outer turning point is higher and, hence, the lobe of the wavefunction closer to the outer turning point is more intense. This is reflected in the structure of the cross-correlation function. Anharmonicity makes the excited-state WP more diffuse and the peaks appearing in $C_{00}(t)$ and $C_{10}(t)$ decrease in height and become wider. The results of σ_A and REP for this system are reproduced in figures 10(*b*) and (*d*) respectively.

5.1.3. *Symmetric double-well excited state*

The WP propagation on the double-well excited state was carried out on a spatial grid $(r_{\min}, \mathrm{d}r, N_r) = (4.0a_0, 0.02a_0, 256)$ for a total of 352.91 fs using $\Delta t = 0.01077$ fs. Both $C_{00}(t)$ and $C_{10}(t)$ are strongly dependent on the height of the double-well barrier.

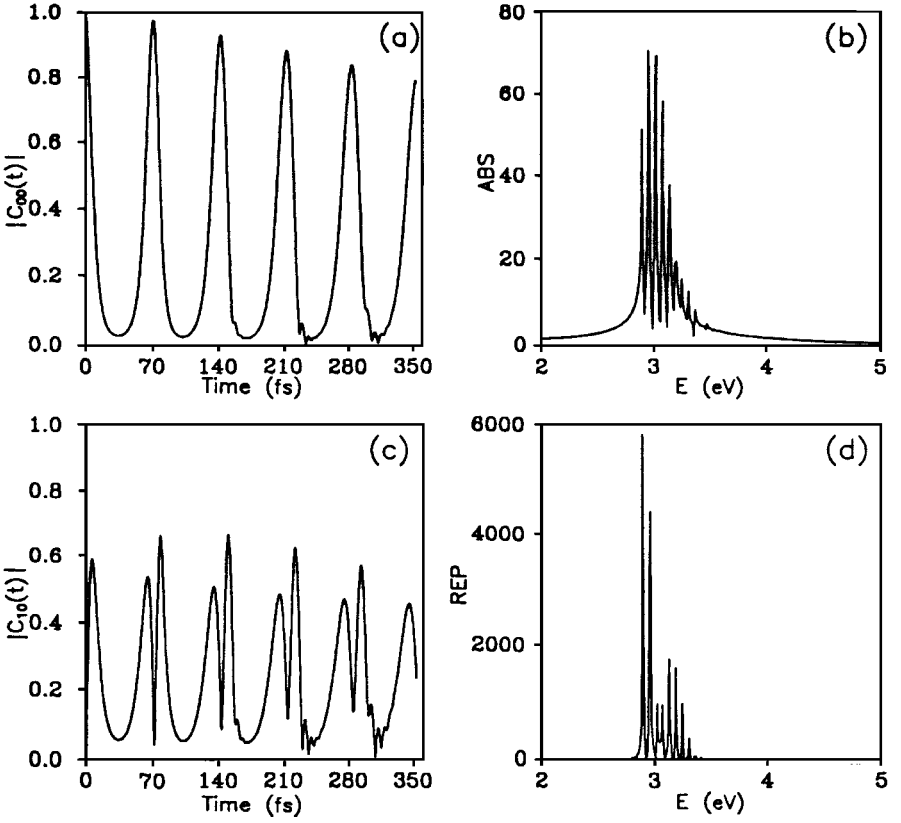

Figure 10. Same as in figure 9 for harmonic-to-Morse excitation.

Some fraction of the WP in one well either crosses over or leaks through the barrier and goes to the other side. Consequently, $C_{00}(t)$ plotted in figure 11(*a*) shows a complex pattern despite the apparent periodicity. $C_{10}(t)$ also becomes quite complicated with increase in time as shown in figure 11(*c*). Both the absorption cross-section and the REP exhibit structures corresponding to the bound states of the double-well potential (see figures 11(*b*) and (*d*)).

5.1.4. *Repulsive excited state*

The WP propagation on the excited state was carried out on a spatial grid ($r_{\min}$, dr, N_r) = ($3.5a_0, 0.05a_0, 256$) for a total of 88.15 fs using $\Delta t = 0.00538$ fs. Because of the nature of the excited state, the WP moves away from the FC region and it never returns! As a result, $C_{00}(t)$ is a monotonically decreasing function and $C_{10}(t)$ has one envelope corresponding to the overlap of the promoted-state wavefunction with the final-state wavefunction, during its passage away from the FC region, towards the asymptote as shown in figures 12(*a*) and (*c*). The absorption cross-section does not show any structure and the REP (referred to as the continuum Raman in this case) is also structureless as illustrated in figures 12(*b*) and (*d*) respectively.

REPs are usually computed by including a phenomenological damping factor in the form of $\exp(-\Gamma t/\hbar)$, multiplying the cross-correlation function (prior to the Fourier transform). The lifetime τ of the excited state, in that case, would correspond to $\hbar/\Gamma$. The model calculations mentioned above have assumed an 'infinite' lifetime

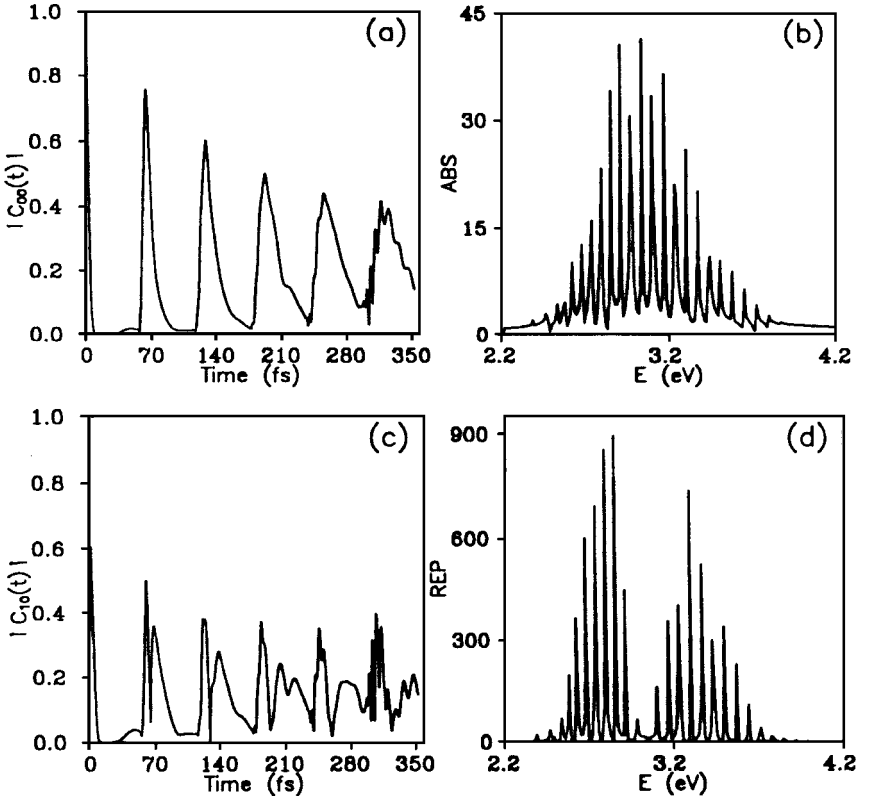

Figure 11. Same as in figure 9 for harmonic-to-symmetric double-well excitation.

($\Gamma = 0$) for the bound excited states. In the case of the dissociative excited states, there is a 'natural' lifetime decided by the slope of the decaying potential. Raman emission is invariably taken to be 'instantaneous'. Therefore, any emission after a few femtoseconds would have to be considered as fluorescence.

For the case of harmonic-to-harmonic photoexcitation, for example, we have examined the influence of the excited-state lifetime on the REP by varying τ from 1 fs to 1 ps. The resulting REPs together with the corresponding $C_{10}(t)$s are plotted in figure 13. It is clear that, when the excited state is short lived ($\tau \approx 1$ fs), the REP shows a single broad hump. With increase in τ to 10 fs, the REP becomes narrower and is also more intense. With further increase in τ (100 fs), additional structures develop. For $\tau = 1.0$ ps the REP is highly structured, revealing the individual vibrational states (accessible) in the excited electronic state.

With increase in τ the REPs become increasingly intense. For $\tau = 0$, there is no resonance Raman, the Raman scattering is weak and the REP is independent of excitation wavelength. For an excited state that lives 'for ever', the REP is highly structured and intense.

We have considered only the Condon approximation ($\mu =$ constant) in the above discussion. It can be expected that μ can vary with r. For a $\mu(r)$ that varies linearly with r in the vicinity of r_e (the equilibrium bond distance in the ground state), we can expect some noticeable changes in $C_{10}(t)$ and hence in the REP.

Much of the theoretical analysis of resonance Raman excitation observed in the laboratory focuses attention on the REP for individual (Raman-active) vibrational

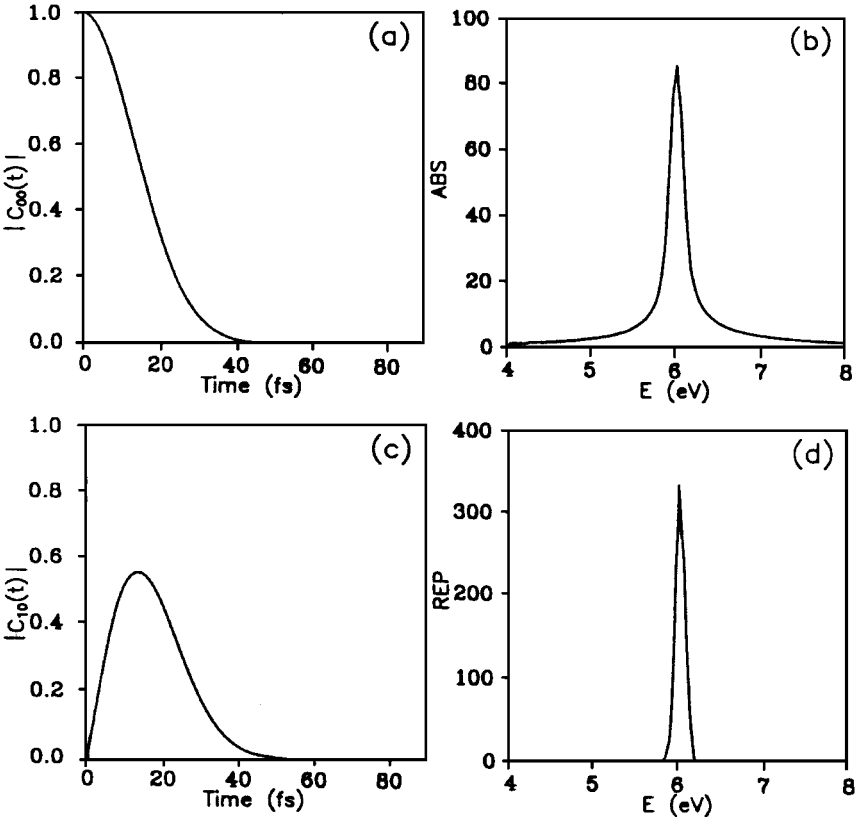

Figure 12. Same as in figure 9 for harmonic-to-dissociative excitation.

modes and it concerns only the relative shift ($\Delta = (r'_e - r_e)/r_e$) in the equilibrium position in going from the ground to the excited state. For example, see [58, 59].

5.2. *Multiple excited states and wave packet interference effects*

For several systems, there is more than one excited electronic state and often they are coupled to each other, in addition to being coupled to the ground electronic state. They are expected to lead to interference between portions of the wavefunction evolving on the different electronic states and result in resonance de-enhancement [60]. Therefore, we have undertaken a model study to investigate the effect of relative location of the curve-crossing with respect to the FC excitation region on the outcome of the dynamical process, that is the population variation with time on the coupled states, autocorrelation and cross-correlation functions, absorption spectrum, REP and relative quantum yields between channels [61].

The Born–Oppenheimer approximation is expected to break down when more than one electronic state approach each other within a vibrational quantum of energy. In dealing with such a situation, one usually resorts to a *diabatic* electronic representation. In this case the states are coupled through the electronic part of the Hamiltonian matrix rather than the nuclear kinetic energy part as in the adiabatic electronic

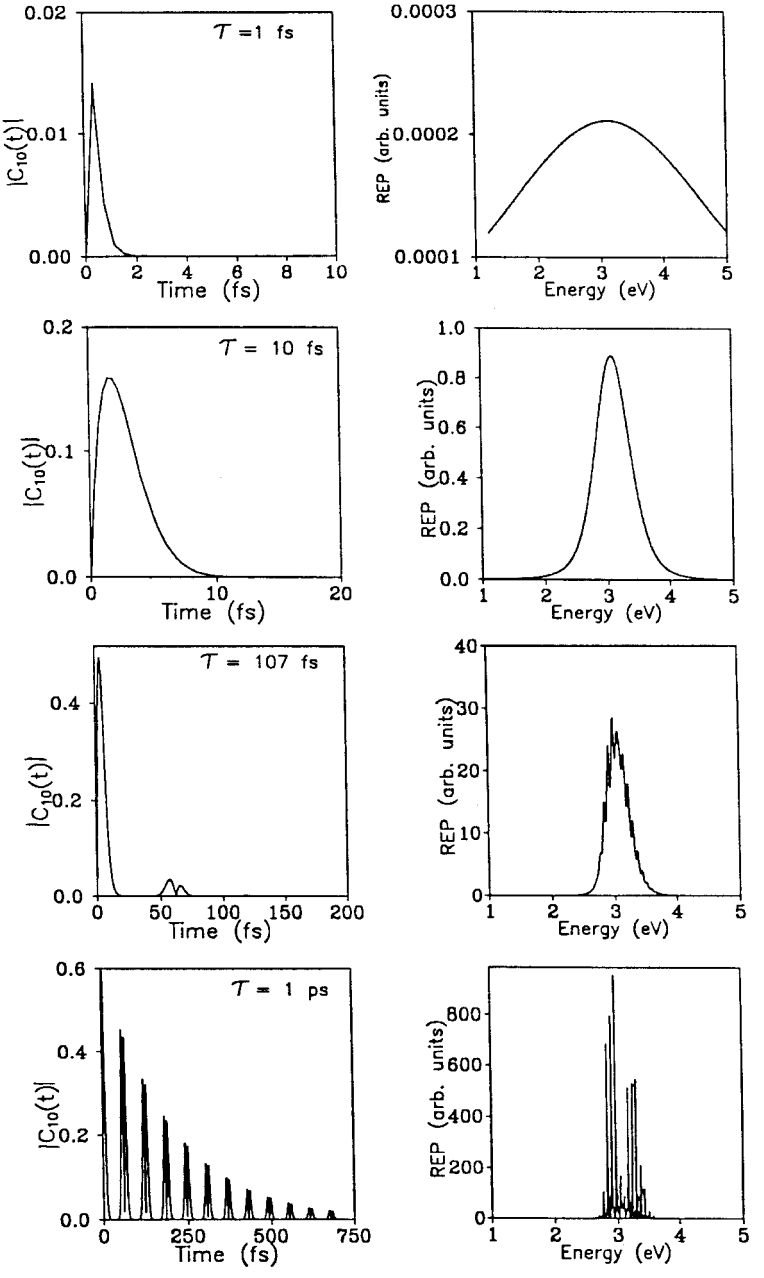

Figure 13. The effect of the excited-state lifetime on the Raman correlation function and the REPs; the excited-state lifetimes τ are indicated.

representation. In the latter case the non-diabatic coupling elements exhibit singularity at the point of degeneracy [62]. Also, the transition dipole matrix elements are quickly varying functions of the nuclear coordinates in the adiabatic representation and the generalized Condon approximation is no longer valid [63].

We have considered three diabatic electronic states for a diatomic molecule. The

Table 2. Parameters for the ground-state and the excited-state potential energy curves, non-adiabatic coupling and for time evolution on the grid.

D_e, α, r_e	2.0 eV, $1.0a_0^{-1}$, $1.4a_0$
a_1, a_2, b_1, b_2	1.6 eV, 1.8 eV, $0.4a_0^{-1}$, $0.5a_0^{-1}$
h_x, β_x	0.03 eV, $5.0a_0^{-2}$
V_{shift}	0.5 eV
r_{min}, dr, N_r	$0.1a_0$, $0.04a_0$, 512
dt, N_t	0.005 38 fs, 32 768

ground state is taken to be a bound state with the potential V_0 represented by a Morse curve

$$V_0(r) = D_e \{\exp[-2\alpha(r - r_e)] - 2\exp[-\alpha(r - r_e)]\}. \tag{27}$$

Two close-lying excited states (both dissociative) are denoted as V_1 and V_2 respectively:

$$V_1(r) = a_1 \exp[-b_1(r - r_1)] + V_{shift}, \tag{28}$$

$$V_2(r) = a_1 \exp[-b_2(r - r_2)], \tag{29}$$

where V_{shift} refers to a constant energy term added to V_1. We use a Gaussian non-adiabatic coupling function V_{12} between the two excited states:

$$V_{12}(r) = h_x \exp[-\beta_x(r - r_x)^2]. \tag{30}$$

The ground state is coupled to the excited states only through radiation (electric dipole interaction). In equation (30) the parameters h_x and β_x define the shape of the Gaussian coupling element and r_x locates the crossing point. We keep the height and width of the coupling function constant in this study as their variation will change the amount of wavefunction transfer between the coupled states and also the time span of the interference effect [64, 65]. For simplicity, the radiation dipole interaction element $\mu \cdot \boldsymbol{E}$ is taken as unity. This means that we impose no particular temporal or spatial shape on the radiation field. We have considered three different points of crossing between the excited states, relative to the FC excitation region. The parameters for the relevant potential energy curves are listed in table 2.

To start with, we consider excitation from the ground vibrational state (v = 0) of the ground electronic state. The initial condition of the promoted-state wavefunction is represented as

$$|\phi^l(0)\rangle = \mu^l |\chi_0\rangle, \quad l = 1, 2, \tag{31}$$

where χ_0 represents the wavefunction of the ground vibronic state, μ is the transition dipole moment and l is the channel index denoting the different excited states. The time evolution of the excited-state wavefunction is governed by the coupled differential equation [32]:

$$i\hbar \frac{\partial}{\partial t}\begin{pmatrix}\phi^1 \\ \phi^2\end{pmatrix} = \begin{pmatrix}H_{11} & V_{12} \\ V_{21} & H_{22}\end{pmatrix}\begin{pmatrix}\phi_1 \\ \phi_2\end{pmatrix}. \tag{32}$$

The symbols H_{ij} and V_{ij} have their usual meanings. The Laplacian of the wavefunction is evaluated using the FFT algorithm and the time evolution is followed using the SOD scheme [6]:

$$\phi^l(t + \Delta t) = \phi^l(t - \Delta t) - \frac{2iH\Delta t}{\hbar}\phi^l(t). \tag{33}$$

The autocorrelation function $C^l_{00}(t) = \langle\phi^l(0)|\phi^l(t)\rangle$ for each excited state l is evaluated at each time step and the total ($C_{00}(t) = \Sigma_{l=1}^{2} C^l_{00}(t)$) is plotted in figure 14(*c*).

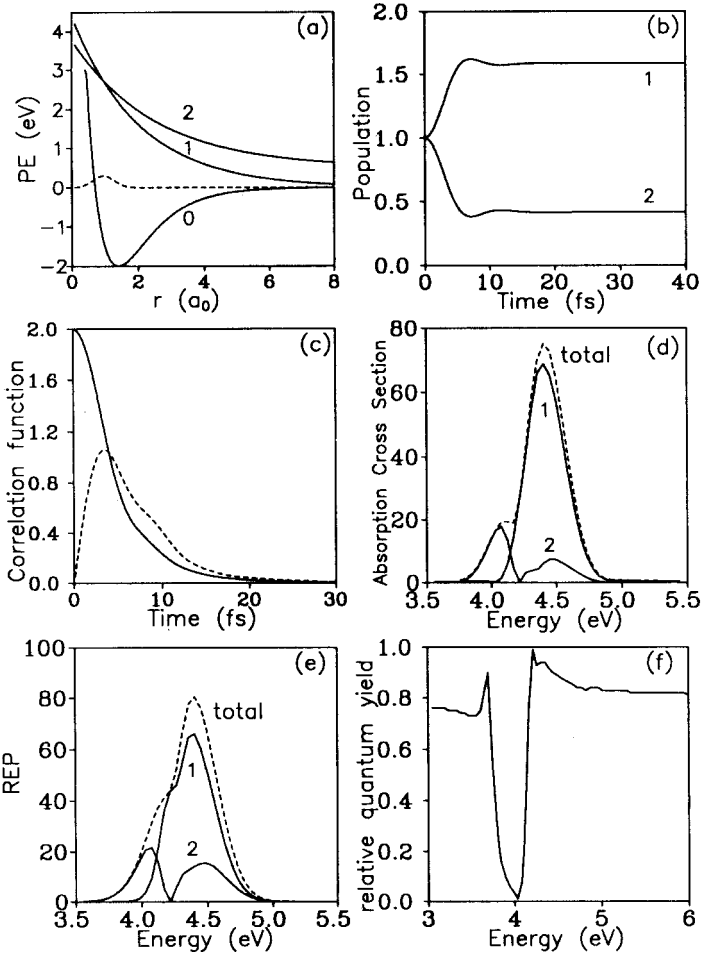

Figure 14. (*a*) The potential energy (PE) curves for the ground state (0) and the two excited states (1 and 2) which cross before the FC point ($r_x < r_e$) ((–––), non-adiabatic coupling); (*b*) the population variation with time; (*c*) the autocorrelation function (——) and cross-correlation function for the fundamental Raman transition (– – –), (*d*) the partial and total absorption cross-sections; (*e*) the individual and total REPs for the two excited states (1 and 2); (*f*) the relative quantum yield for channel 2.

The Fourier transform of $C^{l}_{00}(t)$ yields the partial photoabsorption–dissociation cross-section σ_l for channel l:

$$\sigma_l(\omega) = \frac{2\pi\omega}{3\hbar c}\int_{-\infty}^{\infty} \exp[\mathrm{i}(\omega + \omega_0)t]\ \langle\phi^l(0)\,|\,\phi^l(t)\rangle\,\mathrm{d}t. \tag{34}$$

The relative quantum yield for channel l is defined as $\sigma_l/\Sigma_l\,\sigma_l$.

The Raman amplitude $\alpha^{l}_{10}(\omega)$ for the fundamental vibrational excitation via each electronic channel is obtained from the cross-correlation function $C^{l}_{10}(t) = \langle\phi_1\,|\,\phi^l(t)\rangle$, where ϕ_1 is the promoted state corresponding to the wavefunction χ_1 for the first excited vibrational state (v = 1) of the ground electronic state [20]:

$$\alpha^{l}_{10}(\omega) = \frac{\mathrm{i}}{\hbar}\int_{0}^{\infty} C^{l}_{10}(t)\exp[\mathrm{i}(\omega + \omega_0)t]\,\mathrm{d}t. \tag{35}$$

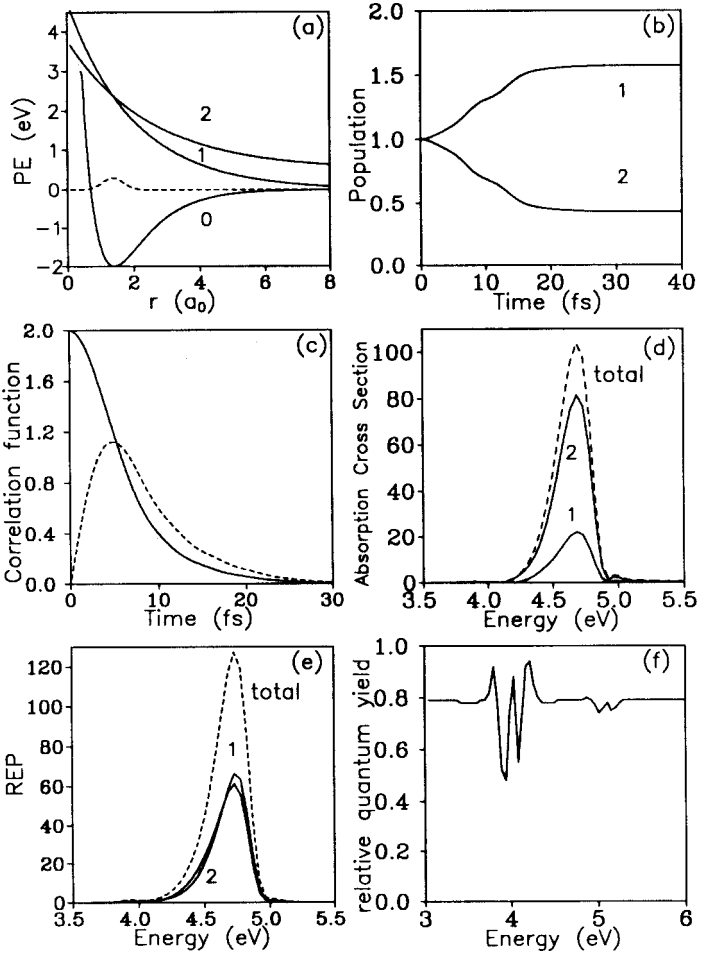

Figure 15. Same as in figure 14 for $r_x = r_e$.

The Raman intensity or the Raman excitation profile for each channel is obtained from the corresponding Raman amplitude:

$$I^{l}_{10}(\omega) = \omega\omega_s^3 |\alpha^{l}_{10}(\omega)|^2. \tag{36}$$

In reality, the observable is the overall Raman excitation profile:

$$I_{10}(\omega) = \omega\omega_s^3 |\alpha_{10}(\omega)|^2, \tag{37}$$

where $\alpha_{10}(\omega) = \Sigma_l \alpha^{l}_{10}(\omega)$. It is clear from the above that there will be constructive and destructive interference between the Raman amplitudes (complex energy domain quantities) for the different channels and the observed REP for the fundamental (as well as the overtone) excitation would reveal enhancement and de-enhancement effects.

5.2.1. *Case A* ($r_x < r_e$)

The parameters specific to the potential energy curves considered in case A are $(r_1, r_2, r_x) = (1.8, 1.8, 0.963)a_0$ respectively. The resulting potential energy curves are shown in figure 14(*a*). The FC transition point is located after the crossing point and the promoted-state wavefunctions come across only the tail of the coupling

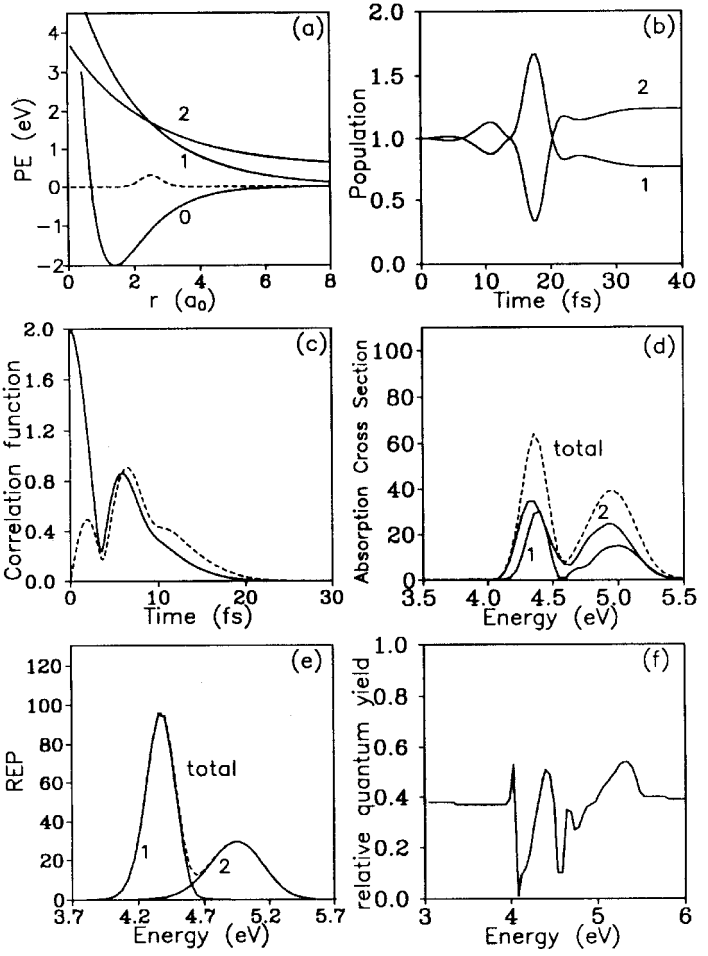

Figure 16. Same as in figure 14 for $r_x > r_e$.

(represented by a Gaussian) region during time evolution. Therefore, there is a transfer of a fraction of the wavefunction from excited state 2 to excited state 1 within the first 5 fs of time evolution, after which the two excited states act as two uncoupled pathways. This is evident from the plots of population as a function of time for each channel in figure 14(*b*). Although the excitation (vertical energy gap) energies are different for the two excited states, their differences fall within the absorption bands of the two states concerned and the interference effect becomes discernible in the absorption cross-section and REP shown in figures 14(*d*) and (*e*) respectively. The relative quantum yield for channel 2, shown in figure 14(*f*), is understandably strongly dependent on energy.

5.2.2. *Case B* ($r_x = r_e$)

The parameters specific to the potential energy curves of case B are $(r_1, r_2, r_x) = (1.8, 1.95, 1.38)a_0$. Here we consider the case when the FC transition point coincides with the crossing point, as shown in figure 15(*a*). The exchange of wavefunctions between the two states starts from the time of excitation and goes on up to 25 fs (see figure 15(*b*)). The very location of the FC point on the curve-crossing region makes the

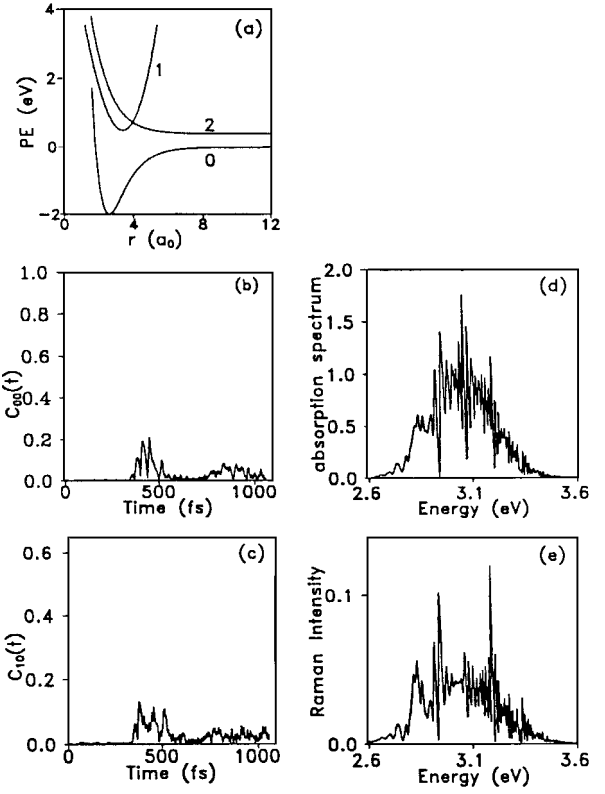

Figure 17. (*a*) The potential energy (PE) curves for a model pre-dissociative system for which the excited state 1 is optically bright; (*b*) the autocorrelation function (starts from unity); (*c*) the cross-correlation function (peaks initially at 0.6); (*d*) the absorption spectrum; (*e*) the Raman intensity.

dynamics highly sensitive to it. The energy ranges for excitation to the two excited states match very well. Hence the absorption cross-sections and the REPs for individual states reinforce each other and no additional hump is observed in the total intensity, as shown in figures 15(*d*) and (*e*). The relative quantum yield for channel 2 varies only moderately over the energy range shown in figure 15(*f*).

5.2.3. *Case C* ($r_x > r_e$)

The parameters specific to the potential energy curves of case C are $(r_1, r_2, r_x) = (1.8, 2.4, 2.51)a_0$. The location of the curve crossing after the FC point (figure 16(*a*)) makes the crossing completely accessible and allows the two promoted-state wavefunctions (evolving on the two excited states) to transfer amplitudes (figure 16(*b*)) up to 35 fs. The velocity of the WP during cross-over, the gradient of the potential energy curves around the crossing point and the mass of the evolving molecule or the molecular fragments are the factors dictating the extent of transfer of the amplitudes between the coupled states. The strength (height and width) of the coupling function is also an important factor. A dip in the total absorption spectrum and Raman intensity appears as shown in figures 16(*d*) and (*e*) since the vertical excitation energies for the two states are significantly different. The relative quantum yield for channel 2 reflects the coupling between the two channels, as illustrated in figure 16(*f*).

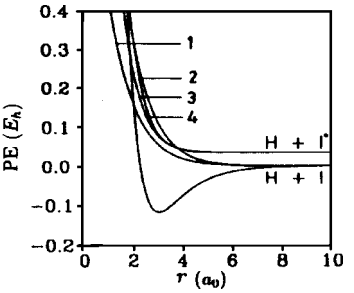

Figure 18. Potential energy curves for HI [66]. Excited states 1, 2, 3 and 4 correspond to $^3\Pi_1$, $^1\Pi_1$, $^3\Sigma_1$ and $^3\Pi_0$ respectively.

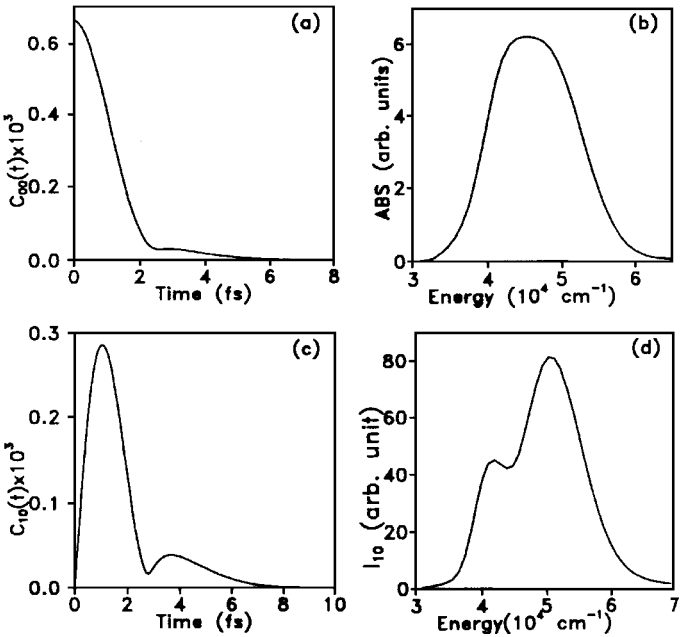

Figure 19. (*a*) The cumulative autocorrelation function, (*b*) the total absorption (ABS) cross-section, (*c*) the cumulative cross-correlation function and (*d*) the total continuum Raman excitation profile for the fundamental Stokes transition for HI [68].

5.2.4. *Further model study*

The three different model cases discussed so far consider two optically bright repulsive excited states and their role in determining the outcome of the photodynamical event as a function of the location of the curve-crossing point. Now we report one more model study in which there are two excited states coupled to each other and only one of them is optically bright. One of them (the optically bright state) is bound in nature and the other is repulsive. That is, this is a model pre-dissociative case and the coupling region is characterized by a Gaussian coupling element centred at the crossing point. Figure 17(*a*) shows the model pre-dissociative system and the correlation functions are shown in figures 17(*b*) and (*c*), whereas the absorption cross-section and REP are shown in figures 17(*d*) and (*e*) respectively. The additional structures in figures 17(*d*) and (*e*) are due to the coupling between the excited states and the envelopes in both the spectra are determined by the early part of the

autocorrelation and cross-correlation functions. The structures that appear in the time correlation functions after 500 fs become reflected in the absorption cross-section and Raman intensity patterns in the form of fine structures.

Considering HI as a realistic example, we have computed the photodissociation cross-section by computing the autocorrelation function [32]. In its first absorption band, HI supports four repulsive excited states and three of them are non-adiabatically coupled to each other, as shown in figure 18 [66]. Two of them lead to the H +H channel and two to H +H*. By choosing the initial vibrational state of HI, we showed that the dissociation channel could be controlled. In figure 19 are plotted the cumulative autocorrelation and cross-correlation functions and also the absorption cross-section and continuum Raman profile for HI [67]. The special point to be noted here is the quantum interference effect in the total Raman intensity, which shows a 'dip' in the profile. This is termed resonance de-enhancement. Elsewhere [68] we have pointed out using the time cross-correlation function approach that DI would show a more pronounced de-enhancement effect. We have used the same approach to ascertain the role of different excited states in deciding the photoexcitation dynamics of IBr [69].

5.3. *Recovery of the cross-correlation function*

As the Raman amplitude $\alpha_{fi}(\omega)$ is a complex quantity, it has an amplitude and phase information associated with it, and only the modulus of the Raman amplitude survives when the REP is computed. The phase information is lost. Reconstruction of the Raman amplitude from the REP, with recovery of the correct phase information, is an interesting problem, as a subsequent Fourier transformation of it would yield the cross-correlation function. In the molecular dynamics literature there have been only two known methods for direct phase recovery until recently, and each had its own limitations. One was the dispersion method due to Albrecht and co-workers [70, 71] and the other was the method of maximum entropy due to Levine and co-workers [72–76]. The former demands analyticity of $\ln[\alpha_{fi}(z)]$ in the right-half complex plane but the latter requires analyticity of $1/\alpha_{f,i}(z)$ in the same domain, where the Raman amplitude has been extended to the complex plane $z = \gamma - i\hbar\omega$, for $\gamma > 0$. Recently, Lee [77] has proposed a new method for phase recovery from the REP and reconstruction of Raman amplitude. In this method, the Raman amplitude, when extended in the complex plane, may have zeros in the right-half complex plane, while both the dispersion method and the maximum-entropy method demand that the Raman amplitude, when extended in the complex plane, should not have any zeros. Maximum-entropy formalism has been used to generate the time cross-correlation function from the observed REP of iodobenzene excited to the B continuum and comparison with the directly computed time cross-correlation function has been made by Remacle *et al*. [74].

An alternative time-frame approach, canonically conjugate to the energy-frame approach, also exists for calculating the REP directly from the absorption cross-section [78]. Lee and Yeo [78] applied the same to real systems, namely carotene and the hexamethylbenzene–tetracyanoethylene complex to obtain the first-order REP from the experimental absorption cross-section values.

6. Summary and conclusion

With the advent of high-speed computers with adequate memory, numerical solution of the time-dependent Schrödinger equation has become quite a practical approach in the last decade or so, particularly for systems with a few degrees of

freedom. Therefore, time correlation functions are increasingly being used to compute dynamical observables and to obtain insight into the dynamics. In this review, we have outlined the basic methodology involved and illustrated their use in determining the bound states of diatomic and triatomic species, in investigating the quasibound states and transition-state resonances in reactive systems and in computing photoabsorption–dissociation cross-sections and REPs, using examples from our own laboratory. Since the TDQM approach allows one to treat the different electronic states on equal footing, we have been able to examine the role of excited electronic states and wavefunction interference effects in influencing the photo-excitation observables, using model systems.

By necessity, such an approach is limited to systems with a small number of degrees of freedom but they are extremely valuable in obtaining insight into the dynamics and in evaluating the reliability of other approximate methods that are used for larger systems.

Acknowledgments

We are grateful to Professor D. C. Clary for his kind invitation to write this review. This study was supported in part by a grant from the Department of Science and Technology, New Delhi.

References

[1] Wang, M. C., and Uhlenbeck, G. E., 1945, *Rev. mod. Phys.*, **17**, 323.
[2] Bloembergen, N., Purcell, E. M., and Pound, R. V., 1948, *Phys. Rev.*, **73**, 679.
[3] Gordon, R. G., 1968, *Adv. magn. Resonance*, **3**, 1.
[4] Heller, E. J., 1978, *J. chem. Phys.*, **68**, 2066, 3891.
[5] Heller, E. J., 1981, *Accts chem. Res.*, **14**, 368.
[6] Mohan, V., and Sathyamurthy, N., 1988, *Comput. Phys. Rep.*, **7**, 412.
[7] Kosloff, R., 1988, *J. phys. Chem.*, **92**, 2087; 1994, *A. Rev. phys. Chem.*, **45**, 145.
[8] Garraway, B. M., and Suominen, K.-A. 1995, *Rep. Prog. Phys.*, **58**, 365.
[9] Kosloff, R., 1996, *Dynamics of Molecules and Chemical Reactions*, edited by R. E. Wyatt and J. Z. H. Zhang (New York: Marcel Dekker).
[10] Balakrishnan, N., Kalyanaraman, C., and Sathyamurthy, N., 1997, *Phys. Rep.*, **280**, 79.
[11] Manz, J., 1997, *Femtochemistry and Femtobiology*, edited by V. Sundström (Singapore: World Scientific).
[12] Zewail, A. H., 1995, *Femtochemistry*, Vols 1 and 2 (Singapore: World Scientific).
[13] Manz, J., and Wöste, L. (editors), 1995, *Femtosecond Chemistry*, Vols 1 and 2 (Weinheim: VCH).
[14] Cohen, L., 1989, *Proc. Inst. Elect. Electron. Engrs*, **77**, 941.
[15] Feit, M. D., Fleck, Jr, J., and Steiger, A., 1982, *J. comput. Phys.* **47**, 412.
[16] Press, W. H., Flannery, W. P., Teukolsky, S. A., and Vetterling, W. T., 1986, *Numerical Recipes* (Cambridge University Press).
[17] Zhang, D. H., and Zhang, J. Z. H., 1996, *Dynamics of Molecules and Chemical Reactions*, edited by R. E. Wyatt and J. Z. H. Zhang (New York: Marcel Dekker).
[18] Dai, J., and Zhang, J. Z. H., 1995, *J. chem. Phys.* **103**, 477.
[19] Kulander, K. C., and Heller, E. J., 1978, *J. chem. Phys.*, **69**, 2439.
[20] Lee, S.-Y., and Heller, E. J., 1979, *J. chem. Phys.*, **71**, 4777; 1982, *ibid.*, **76**, 3035.
[21] Heller, E. J., Sundberg, R. L., and Tannor, D. J., 1982, *J. phys. Chem.*, **86**, 1822.
[22] Sundberg, R. L., and Heller, E. J., 1982, *Chem. Phys. Lett.* **93**, 586.
[23] Dixon, R. N., 1991, *Accts chem. Res.*, **24**, 16.
[24] Schinke, R., 1993, *Photodissociation Dynamics* (Cambridge University Press).
[25] 1993, *J. phys. Chem.*, **97**, 12 427–12 649.
[26] 1994, *Chem. Phys.*, **187**, 1–225.
[27] Henriksen, N. E., 1995, *Adv. chem. Phys.*, **91**, 433.
[28] Ramakrishna, M. V., and Coalson, R. D., 1988, *Chem. Phys.*, **120**, 327.
[29] Mahapatra, S., and Köppel, H., 1998, *Phys. Rev. Lett.*, **81**, 3116.

[30] MYERS, A. B., 1990, *J. opt. Soc. Am.* B, **7**, 1665; 1996, *Chem. Rev.*, **96**, 911; *Acts chem. Res.*, **30**, 519; *J. Raman Spectrosc.*, **74**, 328.
[31] TANNER, J. J., 1990, *J. chem. Educ.* **67**, 917.
[32] KALYANARAMAN, C., and SATHYAMURTHY, N., 1993, *Chem. Phys. Lett.*, **209**, 52.
[33] KALYANARAMAN, C., and SATHYAMURTHY, N., 1994, *Chem. Phys.*, **187**, 219.
[34] MAHAPATRA, S., and SATHYAMURTHY, N., 1995, *J. chem. Phys.*, **102**, 6057.
[35] MAHAPATRA, S., and SATHYAMURTHY, N., 1996, *J. chem. Phys.*, **105**, 10934.
[36] CHAKRABARTI, N., BALASUBRAMANIAN, V., SATHYAMURTHY, N., and GADZUK, J. W., 1995, *Chem. Phys. Lett.*, **242**, 490.
[37] MAITI, B., MAHAPATRA, S., and SATHYAMURTHY, N., 1999 (to be published).
[38] CARRINGTON, A., BUTTENSHAW, J., and KENNEDY, R. A., 1982, *Molec. Phys.*, **45**, 753.
[39] CARRINGTON, A., and KENNEDY, R. A., 1984, *J. chem. Phys.*, **81**, 91.
[40] CARRINGTON, A., MCNAB, I. R., and WEST, Y. D., 1993, *J. chem. Phys.*, **98**, 1073.
[41] GARCIA DE POLAVIEJA, G., FULTON, N. G., and TENNYSON, J., 1994, *Molec. Phys.*, **83**, 361; 1996, *ibid.*, **87**, 651.
[42] MAHAPATRA, S., VETTER, R., ZUHRT, CH., NGUYEN, H. T., RITSCHEL, TH., and ZÜLICKE, L., 1997, *J. chem. Phys.*, **107**, 2930; 1998, *Chem. Phys. Lett.*, **285**, 41.
[43] MAHAPATRA, S., and KÖPPEL, H., 1998, *J. chem. Phys.*, **109**, 1721.
[44] SADEGHI, R., and SKODJE, R. T., 1993, *J. chem. Phys.*, **98**, 9208; 1993, *ibid.*, **99**, 5126.
[45] SKODJE, R. T., SADEGHI, R., KRAUSE, J. R., and KÖPPEL, H., 1994, *J. chem. Phys.*, **101**, 1725.
[46] SADEGHI, R., and SKODJE, R. T., 1995, *J. chem. Phys.*, **102**, 193.
[47] MAHAPATRA, S., SATHYAMURTHY, N., KUMAR, S., and GIANTURCO, F. A., 1995, *Chem. Phys. Lett.*, **241**, 223.
[48] VARANDAS, A. J. C., and YU, H. G., 1996, *Chem. Phys.*, **209**, 31.
[49] BHATIA, P., MAITI, B., SATHYAMURTHY, N., STAMATIADIS, S., and FARANTOS, S. C., 1999, *Phys. Chem. chem. Phys.*, **1**, 1105.
[50] LEVINE, R. D., and KINSEY, J. L., 1991, *Proc. natn. Acad. Sci.* (*USA*), **88**, 11 133; J. Wilkie and P. Brumer, 1991, *Phys. Rev. Lett.*, **67**, 1185.
[51] ALHASSID, Y., and LEVINE, R. D., 1992, *Phys. Rev.* A, **46**, 4650.
[52] HALLAR, E., KÖPPEL, H., and CEDERBAUM, L. S., 1983, *Chem. Phys. Lett.*, **101**, 215.
[53] MAHAPATRA, S., RAMASWAMY, R., and SATHYAMURTHY, N., 1996, *J. chem. Phys.*, **104**, 3989.
[54] ALHASSID, Y., and WHELAN, N., 1993, *Phys. Rev. Lett.*, **70**, 572.
[55] MEHTA, M. L., 1990, *Random Matrices*, second edition (New York: Academic Press).
[56] MAHAPATRA, S., SATHYAMURTHY, N., and RAMASWAMY, R., 1997, *Pramana—J. Phys.*, **48**, 411.
[57] MAHAPATRA, S., 1996, *J. chem. Phys.*, **105**, 344.
[58] BISWAS, N., and UMAPATHY, S., 1995, *Chem. Phys. Lett.*, **236**, 24.
[59] BISWAS, N., UMAPATHY, S., KALYANARAMAN, C., and SATHYAMURTHY, N., 1995, *Proc. Indian Acad. Sci.* (*chem. Sci.*), **107**, 233.
[60] REBER, C., and ZINK, J. I., 1992, *J. phys. Chem.*, **96**, 571.
[61] CHAKRABARTI, N., 1997, PhD thesis, Indian Institute of Technology, Kanpur, India, 1997.
[62] LICHTEN, W., 1963, *Phys. Rev.*, **131**, 229; SMITH, F. T. 1969, *Phys. Rev.*, **179**, 111; O'MALLEY, T. F. 1971, *Adv. at. molec. Phys.*, **7**, 223; PACHER T., CEDERBAUM, L. S., and KÖPPEL H., 1993, *Adv. chem. Phys.*, **84**, 293.
[63] DOMCKE, W., KÖPPEL, H., and CEDERBAUM, L. S., 1981, *Molec. Phys.*, **43**, 851.
[64] RAMAKRISHNA, M. V., 1990, *J. chem. Phys.*, 93, 3258.
[65] GRANUCCI, G., and PERISCO, M. 1995, *Chem. Phys. Lett.*, **246**, 228.
[66] LEVY, I., and SHAPRIO, M., 1988, *J. chem. Phys.*, **89**, 2900.
[67] CHAKRABARTI, N., KALYANARAMAN, C., and SATHYAMURTHY, N., 1997, *Chem. Phys. Lett.*, **267**, 31.
[68] CHAKRABARTI, N., and SATHYAMURTHY, N. 1998, *J. phys. Chem.* A, **102**, 7089.
[69] VANDANA, K., CHAKRABARTI, N., SATHYAMURTHY, N., and MISHRA, M. K., 1998, *Chem. Phys. Lett.*, **288**, 545.
[70] CHAMPION, P. M., and ALBRECHT, A. C., 1981, *Chem. Phys. Lett.*, **82**, 410.
[71] JOO, T., and ALBRECHT, A. C., 1993, *J. phys. Chem.*, **97**, 1262.
[72] REMACLE, F., and LEVINE, R. D., 1993, *J. chem. Phys.*, **98**, 2144.

[73] REMACLE, F., and LEVINE, R. D., 1993, *J. chem. Phys.*, **99**, 4908.
[74] REMACLE, F., LEVINE, R. D., and KINSEY, J. L., 1993, *Chem. Phys. Lett.*, **205**, 267.
[75] REMACLE, F., and LEVINE, R. D., 1996, *J. chem. Phys.*, **104**, 1399.
[76] REMACLE, F., and LEVINE, R. D., 1996, *Dynamics of Molecules and Chemical Reactions*, edited by R. E. Wyatt and J. Z. H. Zhang (New York: Marcel Dekker).
[77] LEE, S.-Y., 1995, *Chem. Phys. Lett.*, **245**, 620.
[78] LEE, S.-Y., and YEO, R. C. K., 1994, *Chem. Phys. Lett.*, **221**, 459.